# Journal of Physics Communications

**PAPER**

CrossMark

# Neutron scattering study of the orientational disorder in potassium cyanide

Guanqun Cai[1] , Anthony E Phillips[1] , David A Keen[2] , Matthew G Tucker[3] and Martin T Dove[4,5]

1   School of Physics and Astronomy, Queen Mary University of London, Mile End Road, London, E1 4NS, United Kingdom
2   ISIS Facility, Rutherford Appleton Laboratory, Harwell Campus, Didcot, Oxfordshire, OX11 0QX, United Kingdom
3   Oak Ridge National Laboratory, Neutron Scattering Division, 1 Bethel Valley Road, Oak Ridge, TN 37831, United States of America
4   Department of Physics, School of Sciences, Wuhan University of Technology, 205 Luoshi Road, Hongshan district, Wuhan, Hubei, 430070, People's Republic of China
5   College of Computer Science and College of Physical Science & Technology, Sichuan University, Chengdu 610065, People's Republic of China

**E-mail:** martin.dove@icloud.com

## Abstract

We report the results of a combined neutron diffraction and total scattering study of the orientational order-disorder phase transitions in potassium cyanide, KCN. The diffraction data are analysed in terms of the spontaneous strains that accompany the phase transitions. The total scattering data are analysed using the Reverse Monte Carlo method, which gives direct access to the distribution of atomic positions and hence molecular orientations in each phase. Incorporating information from diffuse scattering in this way provides a means to measure the coefficients of the orientation distribution function up to almost arbitrarily high orders, and furthermore has the advantage that this function is naturally positive everywhere. The results for the cubic phase show that the distribution of orientations never exceeds 25% difference from an isotropic distribution.

## 1. Introduction

### 1.1. Orientationally disordered crystals

Orientational disorder is a common phenomenon in molecular crystals or inorganic crystals.[6] Often, at least in the first phases found on cooling below the melting point, the disorder is dynamic, with the molecules or molecular ions undergoing rotational motion across a continuous distribution of molecular orientations, or jump rotations between a well-defined set of distinct orientations. Examples range from molecular crystals [1] such as fullerenes [2] to polyatomic ions in metal-organic frameworks [3] and even hemes in proteins [4]. Orientational disorder may lead to anomalous materials properties, such as reversible amorphisation under pressure [5] and giant barocaloric effects [6]. For this reason, understanding orientational disorder in materials plays an important role in understanding and tuning [7] such properties of materials.

One simple and intensively studied case is that of the cyanide ion, $CN^-$, in metal cyanides [8]. $CN^-$ exhibits two types of orientational disorder in metal cyanides. In the cristobalite-like group-12 metal cyanides $Zn(CN)_2$ [9] and $Cd(CN)_2$ [10], the cyanide ions can be treated as electric dipoles with static head-to-tail orientational disorder. Apparently this disorder persists to low temperature in $Zn(CN)_2$, but recently reorientational motion and short-range order have been identified in $Cd(CN)_2$ [10]. On the other hand, in the alkali metal cyanides NaCN, KCN and RbCN with the rocksalt structure, the cyanide molecular ions have a much broader distribution of orientations and show rotational diffusion [11] rather than jump motions [12]. In fact, as we will

---

[6] In the past orientationally-disordered materials were called 'plastic crystals' as a result of their mechanical properties, but the scientific community later preferred the term we use here. However, as orientationally disordered crystals have come back into fashion, sometimes people are rediscovering the older name! For the good reasons why the name 'plastic crystals' was replaced by the name 'orientationally disordered crystals' we choose to work with the latter name.

see below, the first phase transition on cooling after freezing involves ordering of the elastic quadrupole moments rather than of the molecular electrical dipole moments.

## 1.2. Methods to quantify the spatial part of orientational disorder from experiment

The atomic structure of crystals with continuous orientational disorder is not easy to study using conventional methods such as Bragg diffraction, because it is not reasonable to identify discrete sites for the positions of atoms. Instead, the atomic structure must be described in terms of a continuous distribution of molecular orientations. A common approach is to expand these distribution functions in terms of an appropriate basis of 'rotator functions' such as symmetry-adapted spherical harmonics [13, 14]. This process reduces the problem of describing the structure to that of determining the appropriate coefficients for the basis functions, which might be done in analysis of Bragg diffraction data using a standard least-squares refinement of the Bragg diffraction data. However, this method has two related problems. First is that it is only practical to relatively low order, and second, as a consequence the resulting distribution function is not necessarily positive for all possible orientations, although there have been some practical suggestions how to solve this by fitting instead an effective rotational potential [15, 16].

An alternative approach is to analyse a set of large molecular configurations. In the past this typically meant analysis of configurations generated by the molecular dynamics simulation method, but from an experimental approach this is now possible using neutron total scattering data together with the Reverse Monte Carlo (RMC) method [17–19]. One recent example of this technique for studying orientational disorder was an investigation of crystalline adamantane [20], but in this case the molecules were found to be confined to be in either of two preferred orientations rather than with a continuous distribution. If the orientational probability distribution function is expanded in terms of orthonormal functions,

$$P(\Omega) = \sum_{\ell} c_\ell \, K_\ell(\Omega) \tag{1}$$

it follows that the coefficients $c_\ell$ can be calculated directly from the statistical averages $c_\ell = \langle K_\ell(\Omega) \rangle$ evaluated from a set of independent configurations. This is not subject to the problem of only allowing low-order terms and thus can be developed to arbitrary accuracy. To date this approach has never been applied to analysis of orientational disorder from total scattering and RMC data. This analysis will be discussed in more detail below.
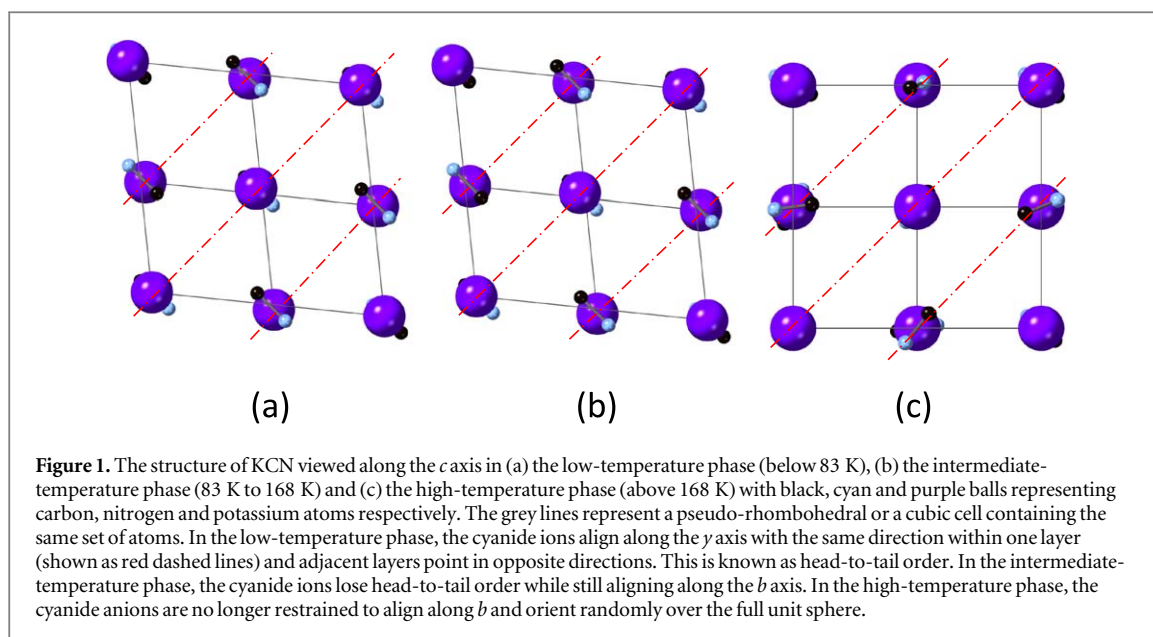
In fact it is now relevant to develop this experimental approach, because some of the new optoelectronic materials that are attracting a lot of interest contain molecular ions such as methylammonium or formamidinium that are free to rotate. One example is the hybrid perovskite solar cell material methylammonium lead iodide (MAPbI$_3$), which has been investigated in a huge number of studies, yet still facing the problem of characterising the orientational disorder from experimental data. MAPbI$_3$ undergoes two phase transitions at ambient pressure involving changes in the degree of orientational order, and it has been shown that these correlate with its temperature-dependent dielectric properties [21]. The methylammonium includes a C–N bond, a direct analogue of the cyanide ion in KCN, for example, and indeed a recent study by molecular dynamics simulation of MAPbI$_3$ compared the ordering to that of KCN from single-crystal diffraction, suggesting that the methylammonium ions are somewhat more isotropic, although again the spherical harmonic expansion was terminated at very low order [22].

For these reasons it is timely to return to the example of KCN. Here we take this material as a case study in the use of the neutron total scattering method to provide information about the distribution of orientations—and hence of electric dipole and elastic quadrupole moments—in an orientationally- disordered or partially-ordered crystal.

## 1.3. The phase transitions in KCN

Below its melting point (907 K), potassium cyanide exists in three distinct crystalline phases [23]. From 168 K up to its melting point, KCN has the well-known rock salt structure with space group $Fm\overline{3}m$ [23, 24]. The cyanide anions occupy sites of the full cubic point symmetry ($m\overline{3}m$) and therefore there is three-dimensional orientational disorder. At 168 K is a phase transition involving considerable but not complete ordering of the cyanide orientations [23]. The crystal structure of this phase is orthorhombic, space group $Immm$. The cyanide anions have their long axes parallel to the orthorhombic [010] axis (equivalent to the $\langle 110 \rangle$ axes in the cubic phase) but with head-to-tail disorder of the electric dipoles [24, 25]. The ordering can be described as involving the molecular elastic quadrupole moments. It is well established that the ordering couples linearly to the softening of the $C_{44}$ shear elastic constant as a result of coupling between the translations and rotations [26–31], meaning that the phase transition is a proper ferroelastic phase transition. At 83 K there is a second phase transition to a fully-ordered structure of orthorhombic space group $Pmnm$ [23, 32]. This has ordering of the electric dipole moments in a proper antiferroelectric arrangement [23, 33].

The atomic structures of the three crystalline phases of KCN are illustrated in figure 1. This figure shows the relationship between the phases, and illustrates the change in orientational ordering.

**Figure 1.** The structure of KCN viewed along the *c* axis in (a) the low-temperature phase (below 83 K), (b) the intermediate-temperature phase (83 K to 168 K) and (c) the high-temperature phase (above 168 K) with black, cyan and purple balls representing carbon, nitrogen and potassium atoms respectively. The grey lines represent a pseudo-rhombohedral or a cubic cell containing the same set of atoms. In the low-temperature phase, the cyanide ions align along the *y* axis with the same direction within one layer (shown as red dashed lines) and adjacent layers point in opposite directions. This is known as head-to-tail order. In the intermediate-temperature phase, the cyanide ions lose head-to-tail order while still aligning along the *b* axis. In the high-temperature phase, the cyanide anions are no longer restrained to align along *b* and orient randomly over the full unit sphere.

## 1.4. Outline of this paper

Although the main thrust of this paper is towards a new quantification of the orientational distribution in KCN, we take a wider look too at the sequence of phase transitions. At the time when KCN was being studied before, there was little opportunity to measure the structure across a wide range of temperatures, and in addition to our total scattering measurements presented here we also consider in more detail than before the nature of the structural changes as a function of temperature. In particular, we can analyse spontaneous strains which give high-precision information about the changes in order, and it seems that until now there are only sketchy reports of the crystal structure of the low-temperature ordered phase.

In the next section we consider the methods we used, both experiment and analysis. We then consider the crystal structure analysis in more detail in section 3. This is followed in section 4 by our analysis of the orientation distribution functions from neutron total scattering and RMC analysis.

## 2. Experimental and analysis methods

### 2.1. Sample

The samples of KCN were obtained commercially from (as then) the Aldrich company. Quoted purity by standard assay was more than 98%, with the largest cited contaminant being Na as a replacement for K at the level of 0.5%. Samples were ground within a glove box in a dry atmosphere, and then immediately loaded into the sample can (see below) whilst still within the glove box.
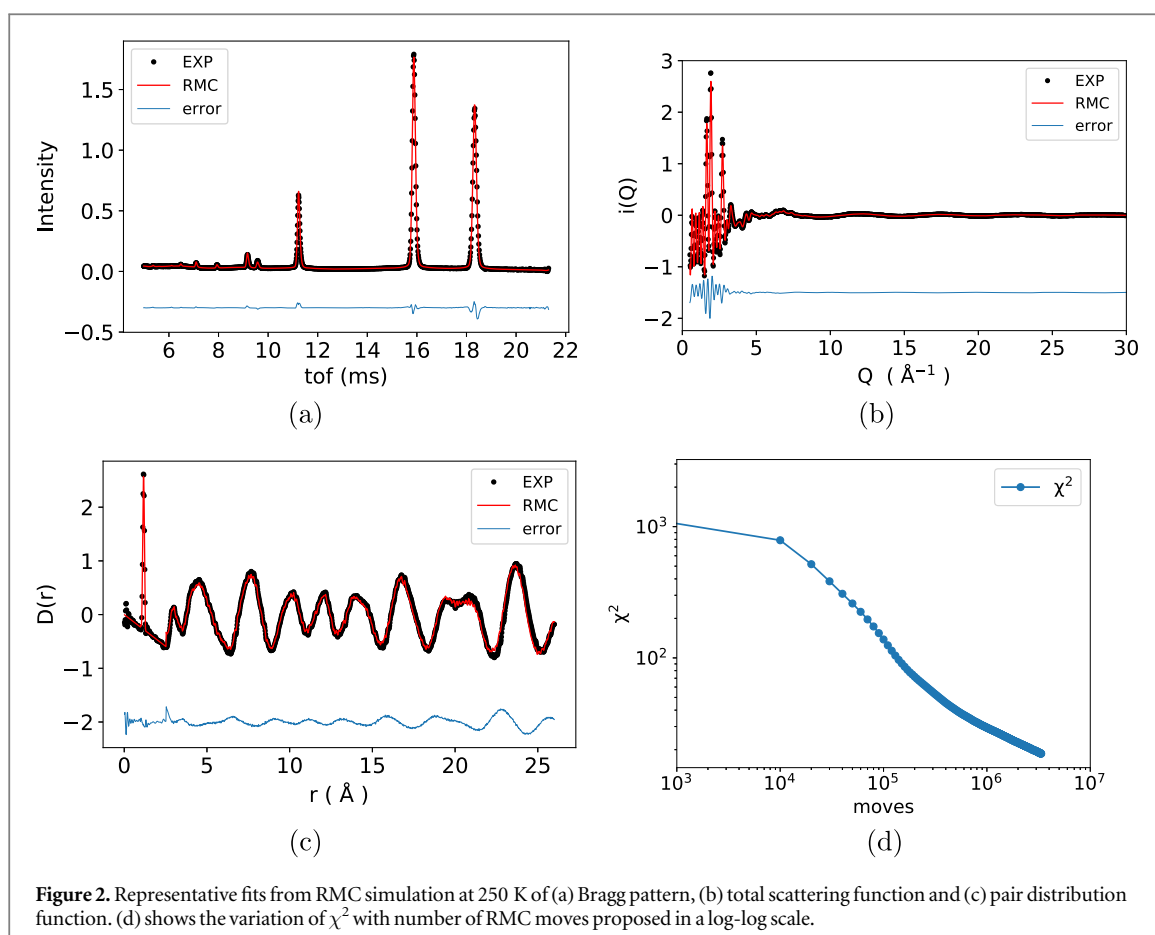
### 2.2. Neutron scattering measurements

Two sets of neutron scattering experiments were performed in this study. A set of neutron powder diffraction measurements were performed using a 10-detector array on the E3 spectrometer/diffractometer on the NRU nuclear reactor at the Chalk River Laboratories [34]. The second set were a combination of neutron diffraction and total scattering measurements performed on the GEM diffractometer at the ISIS pulsed spallation neutron source in the UK [35]. The data from ISIS are publicly available[7]. The data reduction for the NRU data was performed using in-house software, and for the ISIS data using the MANTID software [36].

In both cases the sample was contained within thin-walled vanadium cans. Temperatures were controlled by standard cryostats.

### 2.3. Analysis of diffraction data

The crystal structures of KCN were refined using the the `GSAS/EXPGUI` programs [37–39]. Starting coordinates for the intermediate temperature phase were taken from literature values with disordered occupancy of the C/N sites. For the low-temperature phase the structure was taken as an antiferroelectric ordering of the electric dipole moments of the intermediate-temperature phase. The disordered high-temperature phase has no well-defined positions for the C/N atoms, but nevertheless such positions are

---

[7] The data can be accessed with http://doi.org/10.5286/ISIS.E.RB13786-n (n = 1–7).

**Figure 2.** Representative fits from RMC simulation at 250 K of (a) Bragg pattern, (b) total scattering function and (c) pair distribution function. (d) shows the variation of $\chi^2$ with number of RMC moves proposed in a log-log scale.

required for standard Rietveld analysis and so were selected to lie parallel to the cubic unit cell axes. Backgrounds were fitted using Chebychev polynomials.

### 2.4. Total scattering data and the reverse Monte Carlo analysis

The total scattering data were transformed to the appropriate scattering functions $i(Q)$ and pair distribution functions $D(r)$ using standard procedures; we have described these functions in several previous publications, including one where they are compared with other functions to be found in the literature [40, 47]. The function $D(r)$ is the sine Fourier transform of the scattering function $Qi(Q)$. To extract $i(Q)$ from the scattering data requires account to be taken of the background scattering within the instrument, and the scattering and beam attenuation by the sample container and sample environment. These are obtained in separate measurements, together with a normalisation measurement of a vanadium rod, and the final normalised scattering function $i(Q)$ was formed using the `GUDRUN` package [41, 48].

The Reverse Monte Carlo simulation was performed using the `RMCprofile` code [42]. Configurations of the low-temperature phase used a $12 \times 10 \times 8$ supercell based on the refined crystal structure, set up using the `data2config`/`RMCcreate` code [43]. The configuration for the intermediate-temperature phase was set up in a similar manner, but using an option to randomly rotate the cyanide molecular ions by $180°$ about the normal to the molecular axis. The configuration for the cubic phase was a $8 \times 8 \times 8$ supercell of the cubic phase, using an option to give each cyanide molecular ion a random orientation. The RMC simulations were carried out for 2 315 263 steps in total until convergence (see figure 2(d), giving 70.1 accepted moves per atom and an average move acceptance rate of 18.6%. For each temperature we generated 100 independent configurations for analysis.

## 3. Rietveld analysis of KCN: lattice parameters and spontaneous strain

### 3.1. Crystal structure refinements

The atomic structure of the ordered *Pmnm* phase has atomic coordinates K $\left(\frac{1}{4}, \frac{1}{4} - u_K, \frac{1}{4}\right)$, C $\left(\frac{3}{4}, y_C, \frac{1}{4}\right)$ and N $\left(\frac{3}{4}, y_N, \frac{1}{4}\right)$. The atomic structure of the partially-ordered *Immm* phase has atomic coordinates K $(0, 0, 0)$ and

**Table 1.** Crystal structure data for the low-temperature ordered phase of KCN, space group symmetry *Pmnm* (number 59). Atomic coordinates are of the form $\left(\frac{1}{4}, y, \frac{1}{4}\right)$ for atom type K, and of the form $\left(\frac{3}{4}, y, \frac{1}{4}\right)$ for atom types C and N. These results were obtained by Rietveld refinement of the diffraction data from the GEM diffractometer at ISIS.

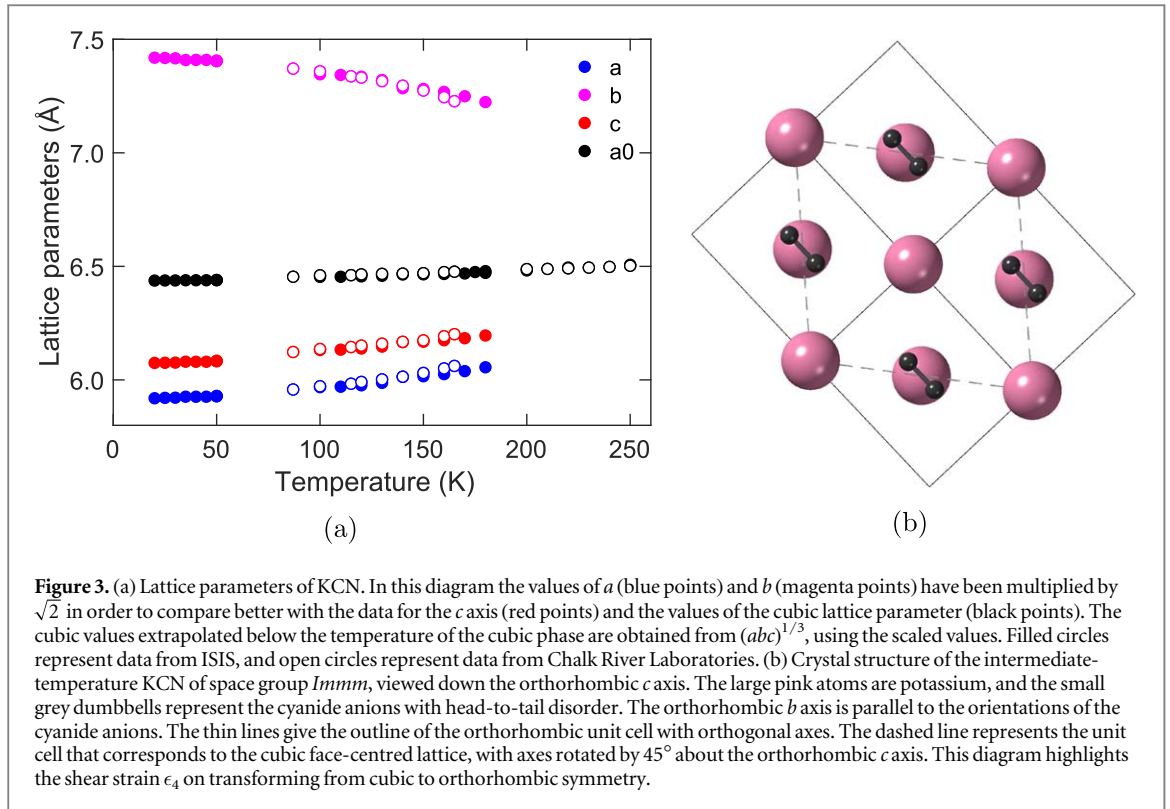| $T$ (K) | $a$ (Å) | $b$ (Å) | $c$ (Å) | atom | $y$ | $U_{11}$ (Å²) | $U_{22}$ (Å²) | $U_{33}$ (Å²) |
|---|---|---|---|---|---|---|---|---|
| 20 | 4.186 31(3) | 5.245 79(5) | 6.074 88(5) | K | 0.2283(4) | 0.87(4) | 1.46(7) | 0.91(4) |
| | | | | C | 0.6418(2) | 1.81(6) | 1.07(6) | 1.21(6) |
| | | | | N | 0.8610(2) | 1.87(4) | 1.39(5) | 1.80(5) |
| 25 | 4.186 70(3) | 5.245 15(5) | 6.075 27(5) | K | 0.2289(5) | 0.99(5) | 1.58(8) | 0.89(4) |
| | | | | C | 0.6417(2) | 1.90(7) | 1.14(7) | 1.13(7) |
| | | | | N | 0.8610(2) | 1.89(5) | 1.38(5) | 1.94(6) |
| 30 | 4.187 18(3) | 5.244 11(6) | 6.076 05(5) | K | 0.2284(4) | 1.05(5) | 1.68(8) | 1.00(5) |
| | | | | C | 0.6418(2) | 1.94(7) | 1.00(7) | 1.36(7) |
| | | | | N | 0.8609(1) | 1.96(5) | 1.55(5) | 1.90(6) |
| 35 | 4.190 26(3) | 5.238 84(5) | 6.080 12(5) | K | 0.2288(5) | 1.20(5) | 1.86(9) | 1.13(5) |
| | | | | C | 0.6427(3) | 2.14(7) | 1.57(9) | 1.37(7) |
| | | | | N | 0.8614(2) | 2.16(5) | 1.33(7) | 2.10(6) |
| 40 | 4.190 18(3) | 5.239 23(5) | 6.079 83(5) | K | 0.2287(4) | 1.10(5) | 1.68(8) | 1.00(5) |
| | | | | C | 0.6418(2) | 2.17(7) | 1.28(7) | 1.38(7) |
| | | | | N | 0.8610(2) | 2.20(5) | 1.60(5) | 2.12(6) |
| 45 | 4.190 27(3) | 5.239 08(5) | 6.079 89(5) | K | 0.2282(4) | 0.97(6) | 1.60(8) | 0.98(5) |
| | | | | C | 0.6424(2) | 2.21(7) | 1.14(7) | 1.49(7) |
| | | | | N | 0.8612(2) | 2.16(5) | 1.71(5) | 2.03(6) |
| 50 | 4.192 49(3) | 5.235 46(5) | 6.083 65(5) | K | 0.2298(4) | 1.14(4) | 1.83(6) | 1.10(4) |
| | | | | C | 0.6420(2) | 2.19(6) | 1.19(6) | 1.34(6) |
| | | | | N | 0.8612(1) | 2.31(5) | 1.82(5) | 2.24(5) |

**Table 2.** Crystal structure data for the intermediate-temperature partially-ordered phase of KCN, space group symmetry *Immm* (number 71). K has atomic coordinates (0, 0, 0). C and N have atomic coordinates of the form $\left(0, y, \frac{1}{2}\right)$, both with occupancy 0.5. These results were obtained by Rietveld refinement of the diffraction data from the GEM diffractometer at ISIS.

| $T$ (K) | $a$ (Å) | $b$ (Å) | $c$ (Å) | atom | $y$ | $U_{11}$ (Å²) | $U_{22}$ (Å²) | $U_{33}$ (Å²) |
|---|---|---|---|---|---|---|---|---|
| 100 | 4.220 03(3) | 5.194 26(5) | 6.131 57(5) | K | — | 2.19(2) | — | — |
| | | | | C/N | 0.110 61(6) | 3.76(2) | 3.15(2) | 2.98(2) |
| 110 | 4.221 39(4) | 5.192 28(6) | 6.133 14(5) | K | — | 2.24(2) | — | — |
| | | | | C/N | 0.110 36(7) | 3.85(2) | 3.21(2) | 3.09(2) |
| 120 | 4.225 76(4) | 5.186 62(7) | 6.138 20(5) | K | — | 2.34(2) | — | — |
| | | | | C/N | 0.110 34(7) | 4.08(2) | 3.33(2) | 3.25(2) |
| 130 | 4.233 41(4) | 5.176 63(6) | 6.146 60(5) | K | — | 2.55(2) | — | — |
| | | | | C/N | 0.109 97(7) | 4.51(2) | 3.50(2) | 3.54(2) |
| 140 | 4.252 04(6) | 5.151 08(10) | 6.165 99(8) | K | — | 2.69(4) | — | — |
| | | | | C/N | 0.109 29(10) | 4.65(4) | 3.36(3) | 3.75(3) |
| 150 | 4.254 04(4) | 5.148 72(7) | 6.167 98(5) | K | — | 2.94(3) | — | — |
| | | | | C/N | 0.108 93(8) | 5.30(3) | 4.10(3) | 4.14(3) |
| 160 | 4.260 60(4) | 5.139 46(8) | 6.174 61(6) | K | — | 3.17(3) | — | — |
| | | | | C/N | 0.108 57(8) | 5.70(3) | 4.33(3) | 4.47(3) |
| 170 | 4.269 92(4) | 5.125 87(8) | 6.183 55(6) | K | — | 3.33(3) | — | — |
| | | | | C/N | 0.107 95(9) | 6.14(3) | 4.65(3) | 4.66(3) |
| 180 | 4.281 94(5) | 5.107 74(10) | 6.195 51(7) | K | — | 3.61(4) | — | — |
| | | | | C/N | 0.107 23(12) | 6.61(4) | 4.93(4) | 5.03(4) |

C/N $\left(0, u, \frac{1}{2}\right)$, with fractional occupancy of 0.5 for both atom types. The atomic structure of the disordered $Fm\bar{3}m$ phase has K (0, 0, 0), and in our refinement we set the coordinates for C/N of the form $\left(\frac{1}{2}, u, 0\right)$ with fractional occupancy of 1/12 for both atom types, as an over-simplified model in order to be able extract lattice parameters. Results for the crystal structure of all three phases refined from the GEM data are given in tables 1–2. We believe that this is the first time that the crystal structure of the *Pmnm* phase has been reported in detail.

### 3.2. Spontaneous strains from the lattice parameters

The variations of the lattice parameters of the cubic and orthorhombic phases with temperature are shown in figure 3(a), using the scaled parameters $a' = \sqrt{2}\,a$ and $b' = \sqrt{2}\,b$ for the orthorhombic phase in order to give values that will tend towards the value of the lattice parameter of the cubic phase. To interpret the lattice

**Figure 3.** (a) Lattice parameters of KCN. In this diagram the values of *a* (blue points) and *b* (magenta points) have been multiplied by $\sqrt{2}$ in order to compare better with the data for the *c* axis (red points) and the values of the cubic lattice parameter (black points). The cubic values extrapolated below the temperature of the cubic phase are obtained from $(abc)^{1/3}$, using the scaled values. Filled circles represent data from ISIS, and open circles represent data from Chalk River Laboratories. (b) Crystal structure of the intermediate-temperature KCN of space group *Immm*, viewed down the orthorhombic *c* axis. The large pink atoms are potassium, and the small grey dumbbells represent the cyanide anions with head-to-tail disorder. The orthorhombic *b* axis is parallel to the orientations of the cyanide anions. The thin lines give the outline of the orthorhombic unit cell with orthogonal axes. The dashed line represents the unit cell that corresponds to the cubic face-centred lattice, with axes rotated by 45° about the orthorhombic *c* axis. This diagram highlights the shear strain $\epsilon_4$ on transforming from cubic to orthorhombic symmetry.

parameters, it is instructive to look at the crystal structure viewed down the orthorhombic *c* axis, figure 3(b). The cyanide anions orient along one of the cubic ⟨110⟩ axes, which corresponds to the orthorhombic *b* axis. This leads to an expansion of the *b* lattice parameter on cooling compared with its value in the cubic phase, with a corresponding reduction in the size of the *a* and *c* axes.

It is striking that the volume of the unit cell appears to show no change in passing through the cubic–orthorhombic phase transition. We can therefore define the parameter $a_0 = (a'\,b'\,c)^{1/3}$, such that $a_0$ acts as the extrapolation of the cubic *a* lattice parameter to low temperature. We define the three axial spontaneous strains as

$$\epsilon_1 = \frac{a' - a_0}{a_0}; \quad \epsilon_2 = \frac{b' - a_0}{a_0}; \quad \epsilon_3 = \frac{c - a_0}{a_0} \tag{2}$$

Their dependence on temperature from the experimental data are shown in figure 4(a).

The axial strains can be combined to create three symmetry-adapted strains [44]. The first is the totally-symmetric volume strain:

$$\epsilon_a = \epsilon_1 + \epsilon_2 + \epsilon_3 \tag{3}$$

The second is the tetragonal strain, namely an expansion along *b* with a shrinkage in the two orthogonal directions:

$$\epsilon_t = \frac{1}{\sqrt{3}}(2\epsilon_3 - \epsilon_1 - \epsilon_2) \tag{4}$$

The third is the shear strain, which in the axial setting of the orthorhombic phase is defined as

$$\epsilon_6 = \epsilon_2 - \epsilon_1 \tag{5}$$

These three strains are shown in figure 4(b). As expected, $\epsilon_a$ is small across the whole range of temperatures. And also, as expected, $\epsilon_6$ is the largest, but $\epsilon_t$ is not insignificant in size.

In figure 5 we show that over the range of the intermediate-temperature *Immm* phase $\epsilon_t \propto \epsilon_6$. This linearity is slightly broken in the low-temperature phase. As will be discussed below, this linear relation is unexpected and unexplained.

### 3.3. Landau free energy function
In order to understand the strain behaviour associated with the phase transition, we obtained the form of the Landau expansion of the free energy associated with the $Fm\bar{3}m$–*Immm* phase transition from the ISOTROPY software [45]:
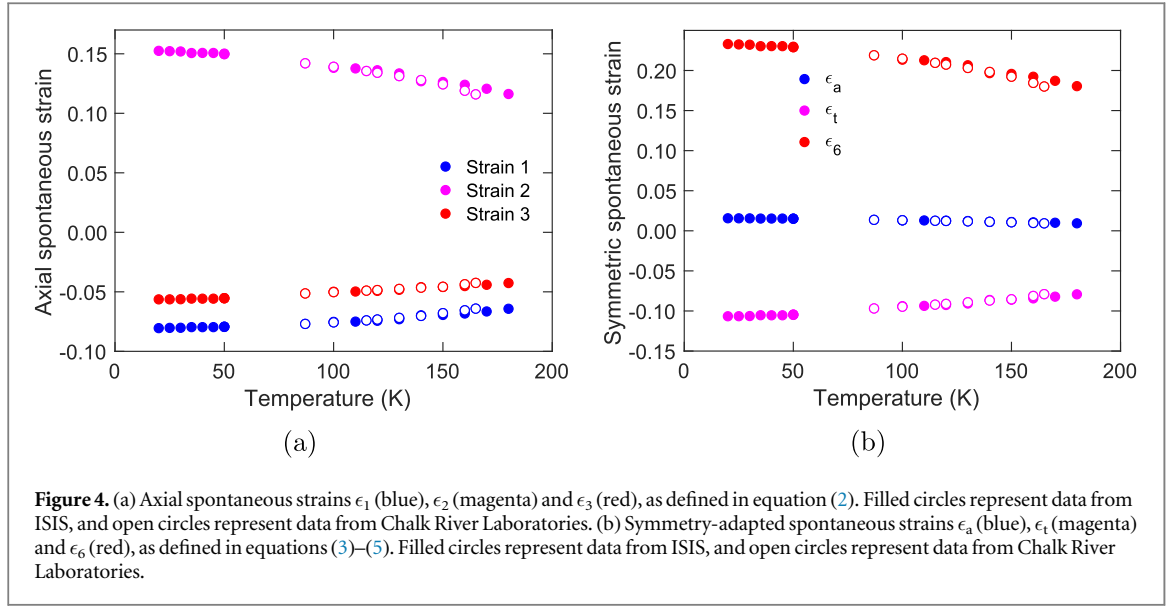
**Figure 4.** (a) Axial spontaneous strains $\epsilon_1$ (blue), $\epsilon_2$ (magenta) and $\epsilon_3$ (red), as defined in equation (2). Filled circles represent data from ISIS, and open circles represent data from Chalk River Laboratories. (b) Symmetry-adapted spontaneous strains $\epsilon_a$ (blue), $\epsilon_t$ (magenta) and $\epsilon_6$ (red), as defined in equations (3)–(5). Filled circles represent data from ISIS, and open circles represent data from Chalk River Laboratories.
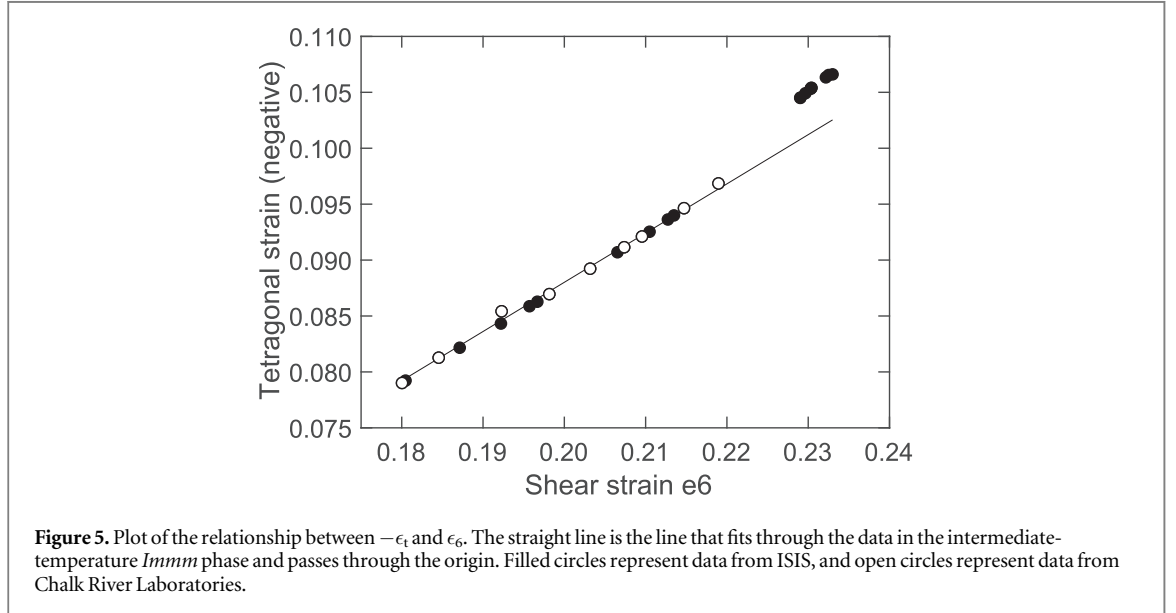


**Figure 5.** Plot of the relationship between $-\epsilon_t$ and $\epsilon_6$. The straight line is the line that fits through the data in the intermediate-temperature *Immm* phase and passes through the origin. Filled circles represent data from ISIS, and open circles represent data from Chalk River Laboratories.

$$G(Q) = \frac{1}{2}a(T - T_0)Q^2 + \frac{1}{4}bQ^4 + \frac{1}{6}cQ^6 + \lambda_6 Q\epsilon_6 + \lambda_a Q^2\epsilon_a + \lambda_t Q^2\epsilon_t$$
$$+ \frac{1}{6}(C_{11}^0 + 2C_{12}^0)\epsilon_a^2 + \frac{1}{4}(C_{11}^0 - C_{12}^0)\epsilon_t^2 + \frac{1}{2}C_{44}^0\epsilon_6^2 \tag{6}$$

where $Q$ is the order parameter, which at this point does not need to be physically defined but will be associated with the orientational order of the cyanide molecular anions. The $C_{ij}^0$ parameters are the bare elastic constants, noting that the actual values of the elastic constants themselves will vary with temperature, including, significantly, a softening of $C_{44}$. At equilibrium, the three strains can be obtained by minimisation of the free energy:

$$\frac{\partial G}{\partial \epsilon_6} = \lambda_6 Q + C_{44}^0\epsilon_6 = 0 \quad \Rightarrow \quad \epsilon_6 = -\frac{\lambda_6}{C_{44}^0}Q \tag{7}$$

$$\frac{\partial G}{\partial \epsilon_a} = \lambda_a Q^2 + \frac{1}{3}(C_{11}^0 + 2C_{12}^0)\epsilon_a = 0 \quad \Rightarrow \quad \epsilon_a = -\frac{3\lambda_\epsilon}{C_{11}^0 + 2C_{12}^0}Q^2 \tag{8}$$

$$\frac{\partial G}{\partial \epsilon_t} = \lambda_t Q^2 + \frac{1}{2}(C_{11}^0 - C_{12}^0)\epsilon_t = 0 \quad \Rightarrow \quad \epsilon_t = -\frac{2\lambda_t}{C_{11}^0 - C_{12}^0}Q^2 \tag{9}$$

(a) K atoms    (b) C atoms    (c) N atoms

**Figure 6.** Representation of the atomic density within a slice of one unit cell viewed down the [001] direction for fractional coordinates $0.4 < z < 0.6$. (a)–(c) shows the atomic density for each atom type at 200 K. Yellow indicates the maximum values of the atomic density, and deep blue indicates the minimum values of the atomic density.
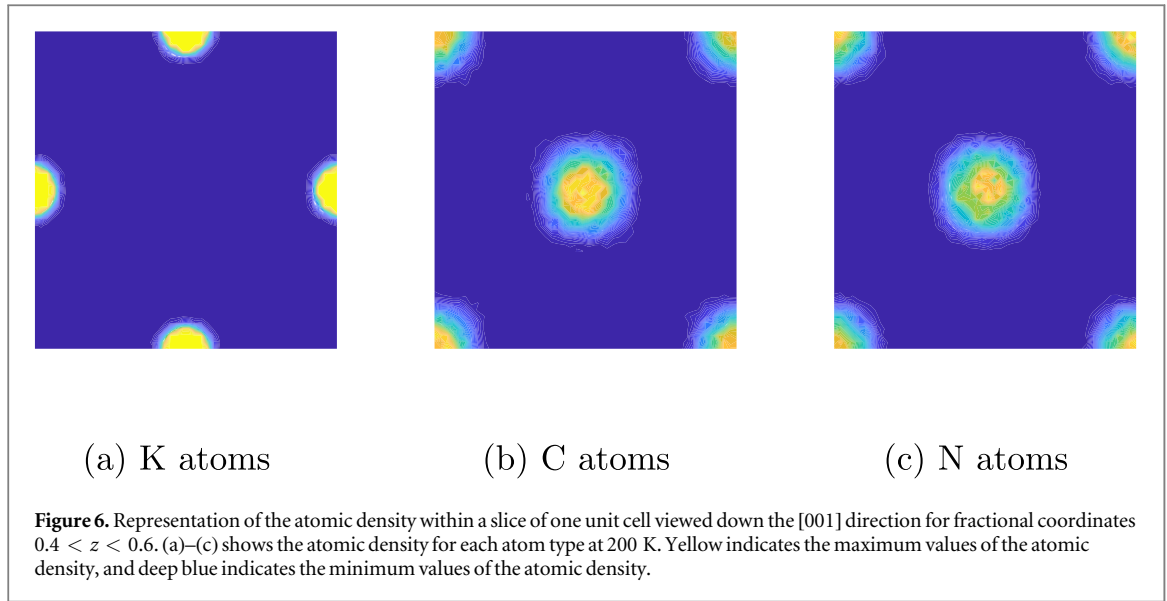
Substitution back into equation (6) gives

$$G(Q) = \tfrac{1}{2}a\left(T - \left(T_0 + \frac{\lambda_6^2}{aC_{44}^0}\right)\right)Q^2 + \left(\tfrac{1}{4}b - \frac{(3/2)\lambda_a^2}{C_{11}^0 + 2C_{12}^0} - \frac{\lambda_t^2}{C_{11}^0 - C_{12}^0}\right)Q^4 + \tfrac{1}{6}cQ^6 \qquad (10)$$

From these equations we see that the linear coupling between the shear strain $\epsilon_6$ and order parameter causes an increase in the phase transition temperature, and that quadratic coupling between the other two strains and order parameter lead to a decreased value of the fourth-order coefficient. The significant size of this coupling leads to the phase transition becoming first-order (discontinuous). The analysis suggests that we expect $-\epsilon_t \propto \epsilon_6^2$, consistent with the fact that $\epsilon_6$ captures the full symmetry change from $Fm\bar{3}m$ to $Immm$ as a proper ferrroelastic phase transition, whereas the strain $\epsilon_t$ would preserve a 4-fold rotation axis in addition to other symmetry operations. This analysis is not consistent with the linear relationship between $\epsilon_6$ and $-\epsilon_t$ seen in the experimental data, figure 5; it is not at all clear to us how such a clear linear relationship can exist.

## 4. Orientational order and local atomic structure from neutron total scattering and RMC simulation

### 4.1. Atomic distributions
The spatial distribution of individual atoms in the unit cell was constructed by collapsing each configuration onto one unit cell, and merging the results from many independent RMC simulations. Figures 6(a)–(c) shows the density profile for each atom type at the cubic phase. Figure 6(a) reflects the large amount of thermal motion of the K atom as seen in the size of the atomic displacement parameter from the Rietveld analysis, table 2. The distribution of C and N atoms is wider in extent. What is interesting from figures 6(b) and (c) are that the distribution of C and N atoms are centred in the middle of the unit cell, rather than the distribution of C and N atoms forming a spherical shell. Thus the orientational disorder is accompanied by a high degree of translational disorder.

The corresponding atomic distributions for the intermediate-temperature (100 K) partially-ordered *Immm* phase are shown in figures 7(a)–(c), and for the low-temperature (20 K) ordered *Pmnm* phase in figures 7(d)–(f). The reduction in translation disorder is clear, and now we see also the distinct sites for C and N atoms. In the intermediate phase there is head-to-tail disorder of the cyanide molecular ions, which is clearly seen in the distribution of C and N atoms.

### 4.2. Information from pair distribution functions
The partial PDFs $g(r)$ for K–K, K–(C/N) and (C/N)–(C/N) are shown in figures 8–10 respectively. For the K–K PDF (figure 8), the high-temperature data show broad peaks at positions consistent with the face-centred cubic arrangement of ions, and in the lower-temperature phases the transition to the orthorhombic phases results in the splitting of these peaks, with the positions being very similar in the two orthorhombic phases but with the expected sharpening of the peaks on cooling through the phase transition from 100 K to 10 K. The peaks up to a distance of around 7 Å in the PDF for the two lower-temperature phases correspond to peaks in the PDF of the high-temperature phase, with the expected broadening, but after 7 Å the peaks positions of the cubic phase are
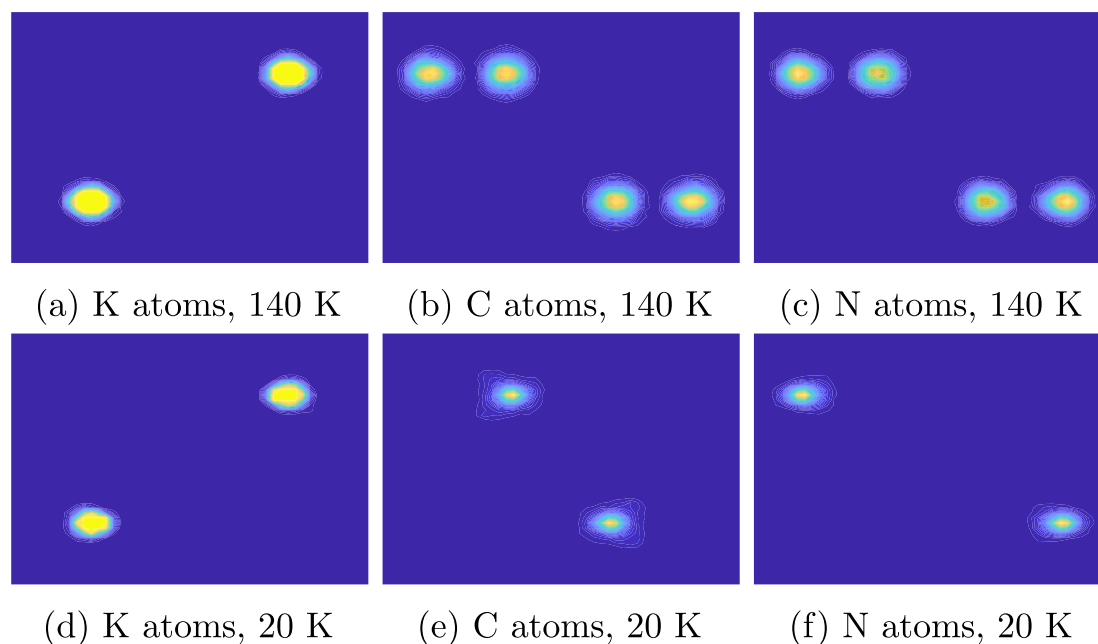
**Figure 7.** Representation of the atomic density within a slice of one unit cell viewed down the [001] direction for fractional coordinates $0.4 < z < 0.6$. (a)–(c) shows the atomic density for each atom type at 140 K. Yellow indicates the maximum values of the atomic density, and deep blue indicates the minimum values of the atomic density. (d)–(f) shows the atomic density for each atom type at 20 K.
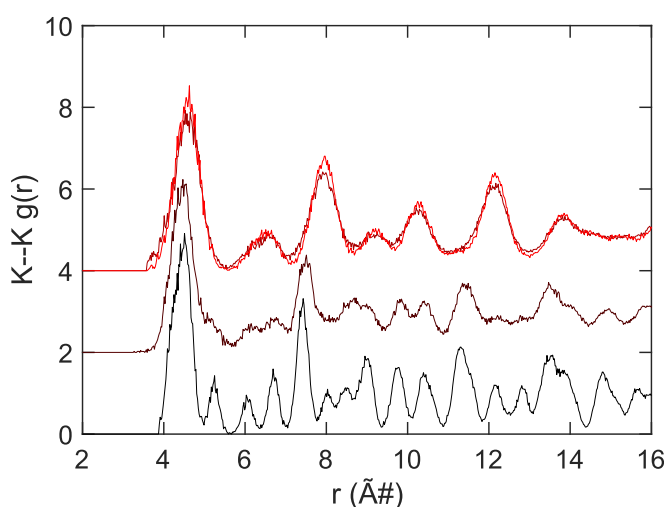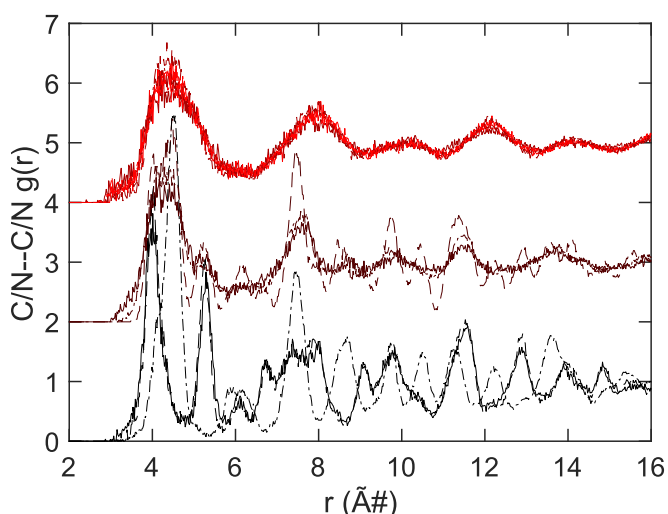


**Figure 8.** K–K partial PDF $g(r)$ for temperatures 20 K (black), 100 K (dark red), 200 K (intermediate red) and 250 K (red), with vertical displacement to separate the results for the different phases.

clearly out of register with those in the orthorhombic phases, reflecting the change in symmetry. The first peak in the PDF of the orthorhombic phase is actually comprised of three peaks, at mid-point distances of around 4.2, 4.4 and 4.6 Å. The first peak in the PDF of the cubic phase is centred on position $a/\sqrt{2}$, and it is broad to the extent that it encompasses the distribution of peaks in the low-temperature phases. The second distinct peak in the PDF for the data at 10 K becomes a shoulder in the data for 100 K, and is subsumed within the tail of the first peak in the cubic phase. The fact that the first peak in the PDF of the cubic phase encompasses the distribution of peaks within the low-temperature orthorhombic peaks suggests that there are local distortions of the unit cell that reflect the local orientations of the CN molecular anions. The same can be said of the second peak too,

The K–C and K–N $g(r)$ results (figure 9) for 10 K show two peaks at around 3.1 and 3.8 Å, which correspond to two cases in which the K atom lies equidistant from both atoms in the CN molecular anion and where the K.. CN and K...NC connections are almost straight lines. It is interesting that we see the same basic form of this $g(r)$ for the cubic phase too for both the same first pair of peaks and beyond, albeit with expected broadening. Clearly
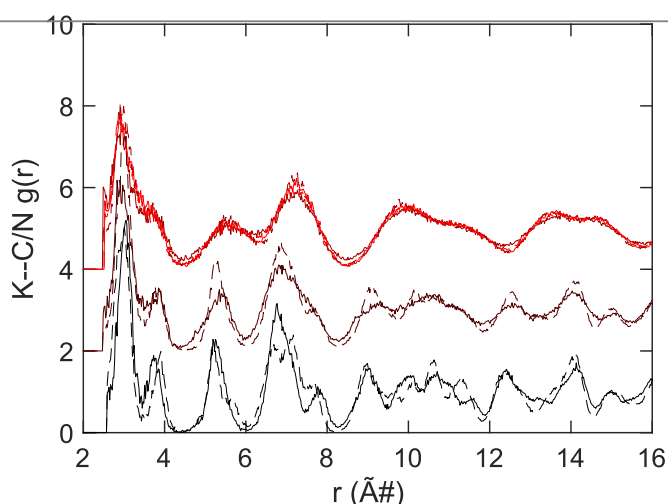
**Figure 9.** K–C (solid lines) and K–N (dashed lines) partial PDF g(r) for temperatures 20 K (black), 100 K (dark red), 200 K (intermediate red) and 250 K (red), with vertical displacement to separate the results for the different phases.



**Figure 10.** C–C (solid lines), N–N (dashed lines) and C–N (dash-dot lines) partial PDF g(r) for temperatures 20 K (black), 100 K (dark red), 200 K (intermediate red) and 250 K (red), with vertical displacement to separate the results for the different phases. For clarity we have excluded the bonded C–N neighbours within the cyanide anion.

the first peak should be the same because it is the nearest-neighbour contact between a K atom and either a C or N atom, but it is interesting that the second peak remains into the high-temperature disordered phase, but broadened and with a midpoint shifted to lower distance. The remaining peaks for the cubic phase are consistent with the positions expected for the cation–anion distance in the rocksalt structure with broadening due to the orientational disorder of the cyanide anions.

The C–C, C–N and N–N $g(r)$ results are shown in figure 10. For the cubic phase, there is no difference between C and N, reflecting the orientational disorder, and the $g(r)$ function for both is similar to that for the K–K $g(r)$ (figure 8) with broadening of peaks reflecting the orientational disorder. In the low-temperature phase, the C–C and N–N distributions are almost identical, and due to the ordering these are not the same as the C–N distribution.

### 4.3. Molecular orientational distribution function

As the simplest type of molecule possible, the cyanide molecular anions consist of only two atoms and therefore containing only one chemical bond. The orientational distribution can be described quantitatively by the bond orientational distribution function $P(\Omega)$. Here $\Omega$ represents the polar angles $(\theta, \phi)$, where $\theta$ is the zenith angle $(0 \leqslant \theta \leqslant \pi)$ and $\phi$ is the azimuthal angle $(0 \leqslant \phi \leqslant 2\pi)$. $P(\Omega)$ describes the probability of a C–N bond lying within a given element of solid angle $d\Omega = \sin\theta \, d\theta \, d\phi$.

We expand $P(\Omega)$ in an orthonormal basis of 'rotator functions' $S_i(\Omega)$:

$$P(\Omega) = \sum_i c_i S_i(\Omega) \tag{11}$$

where the $S_i$ are themselves linear combinations of spherical harmonics $Y_\ell^m(\Omega)$ [31]. It will always be convenient to take real combinations such as

$$Y_\ell^{m,c}(\Omega) = \tfrac{1}{\sqrt{2}}((-1)^m Y_\ell^m(\Omega) + Y_\ell^{-m}(\Omega)) \qquad m > 0 \tag{12}$$

where the 'c' refers to the fact that this function is proportional to $\cos(m\phi)$ [8] [46]. Further combinations may be required, and particular values of $m$ and $\ell$ excluded altogether, depending on the molecular site symmetry. Here we give only a brief explanation of the mathematics relevant to this particular system; full details for all crystallographic point groups are tabulated in the reference by Bradley and Cracknell [46]. With appropriate normalisation applied, we have $c_0 = 1$.

In the low-temperature *Pmnm* phase of KCN, the cyanide ions occupy sites of *mm2* point symmetry. The appropriate functions $S_i(\Omega)$ are $Y_\ell^{m,c}(\Omega)$ with even values of $m$. In the intermediate-temperature *Immm* phase, the point symmetry is *mmm*, and we again take a basis of $Y_\ell^{m,c}(\Omega)$ but now require both $m$ and $\ell$ to be even. Finally, in the high-temperature $Fm\bar{3}m$ phase, the cyanide molecular anions are on sites of $m\bar{3}m$ point symmetry. The relevant basis terms are linear combinations of $Y_\ell^{m,c}(\Omega)$ for various $m$ values, where $\ell$ must be even but the $\ell = 2$ term is also forbidden by symmetry. These functions are known as the Kubic harmonic functions, and are tabulated in the literature in Cartesian form as well as in terms of the spherical harmonics [14, 47], and are given for convenience in the appendix.

As noted earlier, the coefficients in the bond orientational distribution function can be obtained directly by forming the average value of the relevant harmonic from the RMC configurations, in contrast to fitting to data as in diffraction experiments [14]. Here we can compare the calculated distribution function directly with that formed from histograms of bond orientations in the configurations. The form of $P(\Omega)$ for the disordered cubic phase for two arcs of $\Omega$ are shown in figures 11(a) and (b) for temperatures 200 K and 250 K respectively. These show the function calculated from the histogram and from the form of $P(\Omega)$ of equation (1). Values of the coefficients $c_\ell$ were evaluated from averaging over around 100 independent configurations, and are given in table 3, and compared to values obtained from molecular dynamics simulations [25]. All values are small compared with $c_0 = 1$, indicative of a high degree of disorder as seen in figures 11(a) and (b), where the fluctuations from the uniform value $P(\Omega) = 1/4\pi$ do not exceed 10%. There is a very slight preference for ordering along the cubic $\langle 100 \rangle$ directions, and a very slight preference away from the $\langle 111 \rangle$ directions, with no obvious preference for the $\langle 110 \rangle$ directions, the directions in which the cyanide molecular anions order in the two lower-temperature orthorhombic phases. The results appear to show a slightly less uniform distribution at 250 K than at 200 K, but the difference is very small and may not be significant. The RMC results for the coefficients $c_\ell$ are similar to those from the simulations [25], particularly in so far as the coefficients for $\ell > 0$ are remarkably small. Although the coefficients determined by a single-crystal neutron diffraction study [48] presented in table 3 appear slightly different—albeit with a relatively high error—the bond orientational distribution function has some similarities to the results presented here but with larger variance from uniform distribution.

The coefficients for the low-temperature *Immm* phase at 20 K and 50 K, and for the intermediate-temperature *Pmnm* phase at 100 K and 140 K, are given in tables 4 and 5 respectively. The bond orientation functions are shown in figure 12, showing a much higher degree of orientational order as expected. The degree of orientational order/disorder described by the orientation distribution function of each phases is highlighted by calculating the three-dimensional representations as shown in figure 13, together with views of representative RMC configurations.

The picture that emerges from this analysis is that there is almost uniform distribution of orientations of the cyanide anions in the high-temperature cubic phase. The small preference for or against particular orientations is only of order of 10% of the uniform distribution. On the other hand, we see a much greater degree of quadrupolar ordering (that is orientational ordering of the bond ignoring the direction of the dipole moment) in the lower-symmetry phases, and complete ordering on the low-temperature phase. Furthermore, in the low-temperature phase the widths of the distribution function reflect and increase in librational motion on heating from 20 K to 100 K.

---

[8] We follow the results and notation of Bradley and Cracknell [46], but note that since they do *not* include the Condon-Shortley phase factor in their definition of $Y_\ell^m(\Omega)$, neither do they need or include the factor of $(-1)^m$. The equation is given here in the form that we believe will be most useful to a modern reader; in particular this form is compatible with the spherical harmonic functions built in to most popular scientific computing systems, including Mathematica and the SciPy Python library, and with the International tables for Crystallography.
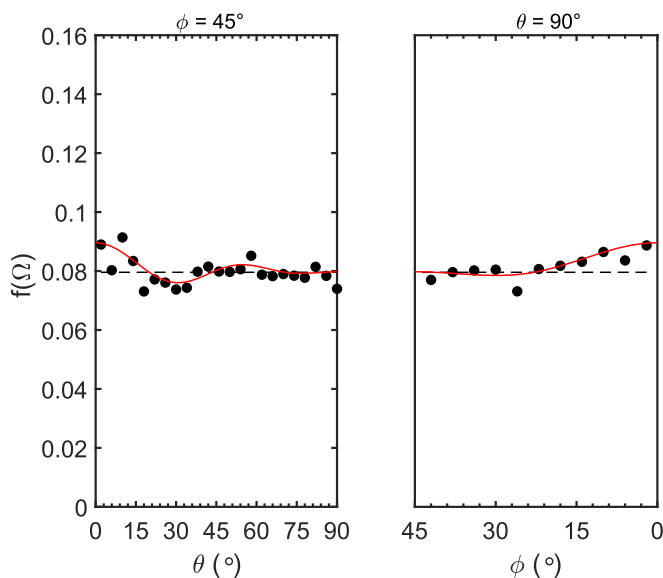
(a) Bond orientation distribution for KCN at 200 K.
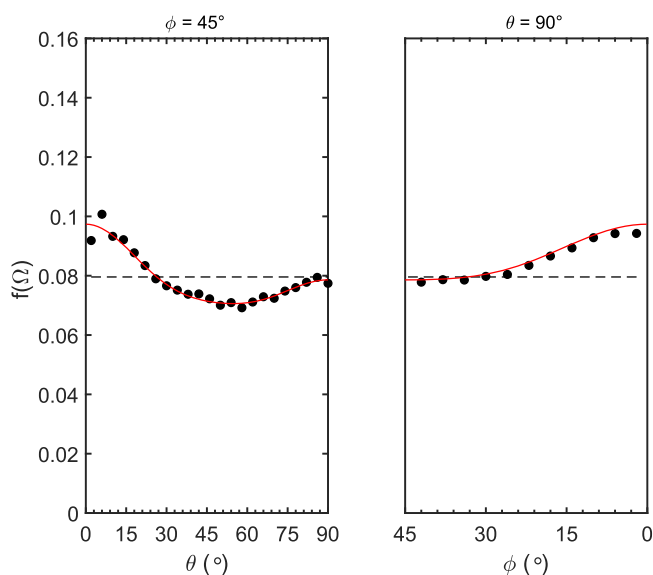


(b) Bond orientation distribution for KCN at 250 K.

**Figure 11.** Bond orientation distribution function for the CN molecular anion in KCN at two temperatures in the disordered cubic phase at two temperatures, a) 200 K and b) 250 K. In both cases the points represent averages from many RMC configurations, and the red lines are calculated from the Kubic harmonic expansion with coefficients calculated from the configurations. The left panels show orientations in the directions from $\langle 001 \rangle$ to $\langle 110 \rangle$, and the right panels show the directions from $\langle 110 \rangle$ to $\langle 100 \rangle$. The broken black line at $f(\Omega) = 1/4\pi$ shows the value for a uniform distribution.

## 5. Conclusions

In this paper we have used neutron scattering methods—Bragg scattering analysed by the Rietveld method, and total scattering analysed by the Reverse Monte Carlo method—to study the orientational- ordering phase transition in KCN in more detail than was previously possible. Bragg scattering has primarily given information about the lattice parameters, which in turn give information on the spontaneous strains that accompany the phase transitions. The strains are coupled to each other and to the degree of order as determined by the symmetry of the free energy function, enabling us to quantify the change in the degree of order within the intermediate and low-temperature phases. That said, there is a linear relationship between the shear and the tetragonal strain that is very difficult to understand.

The orientational order in each phase of KCN has been evaluated from the atomic configurations generated by the RMC method. We have shown that the distribution of orientations of the CN bonds does not vary significantly from random, with the largest deviation being around 25% in favour of orientations in the cubic $\langle 100 \rangle$ directions and showing a reduction of similar size in the $\langle 111 \rangle$ directions. We were able to obtain good

**Table 3.** Calculated values of the coefficients $c_\ell$ of the Kubic harmonic expansion of the bond orientation distribution function $P(\Omega)$ defined in equation (1). RMC results are compared with values calculated in a molecular dynamics simulation [25] and single crystal neutron diffraction study (SCND) [48].

| Method and $T$ (K) | $c_4$ | $c_6$ | $c_8$ | $c_{10}$ |
|---|---|---|---|---|
| RMC 200 | 0.019(2) | 0.013(2) | 0.024(2) | −0.004(3) |
| RMC 250 | 0.079(2) | −0.003(2) | 0.016(2) | 0.000(2) |
| MD 184 | 0.04 | 0.12 | — | — |
| MD 287 | 0.03 | 0.06 | — | — |
| SCND 180 | −0.018(16) | 0.22(14) | — | — |
| SCND 295 | −0.132(22) | 0.23(18) | — | — |

**Table 4.** The values of the coefficients for the $m = 0$ spherical harmonics terms in the bond orientational distribution function for the RMC configurations of the low-temperature *Pmnm* phase of KCN. By normalisation $c_0 = 1$.

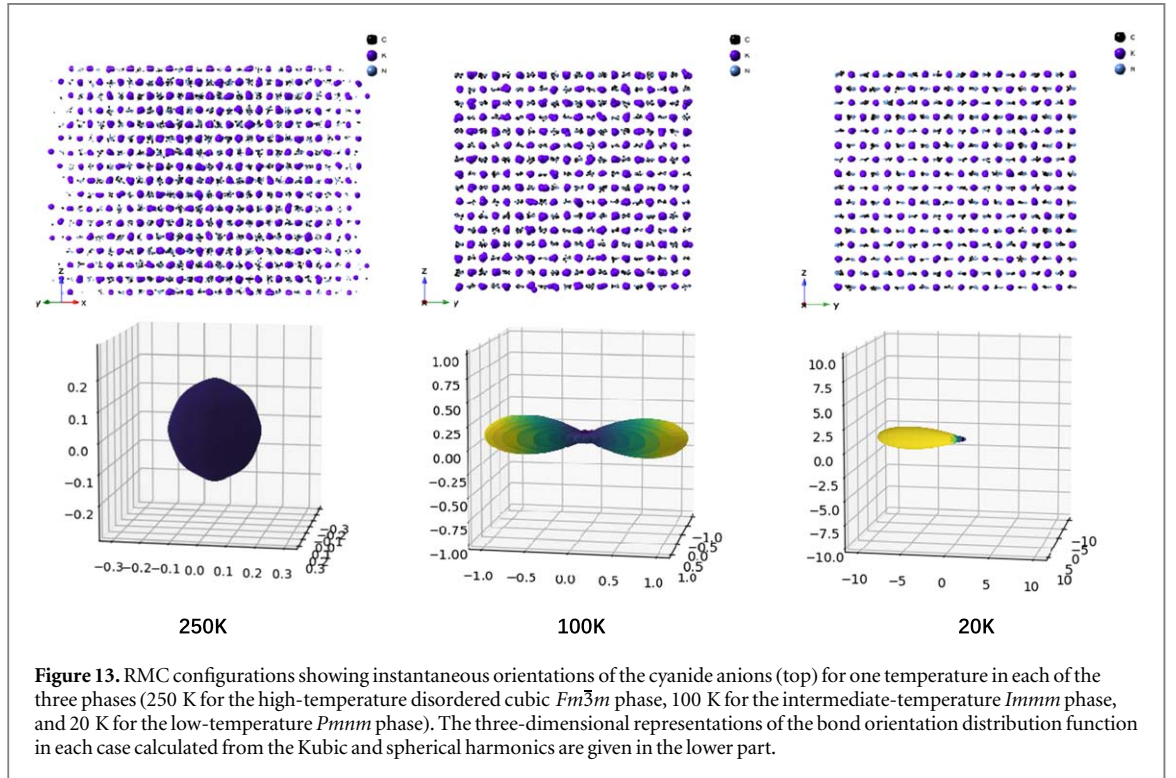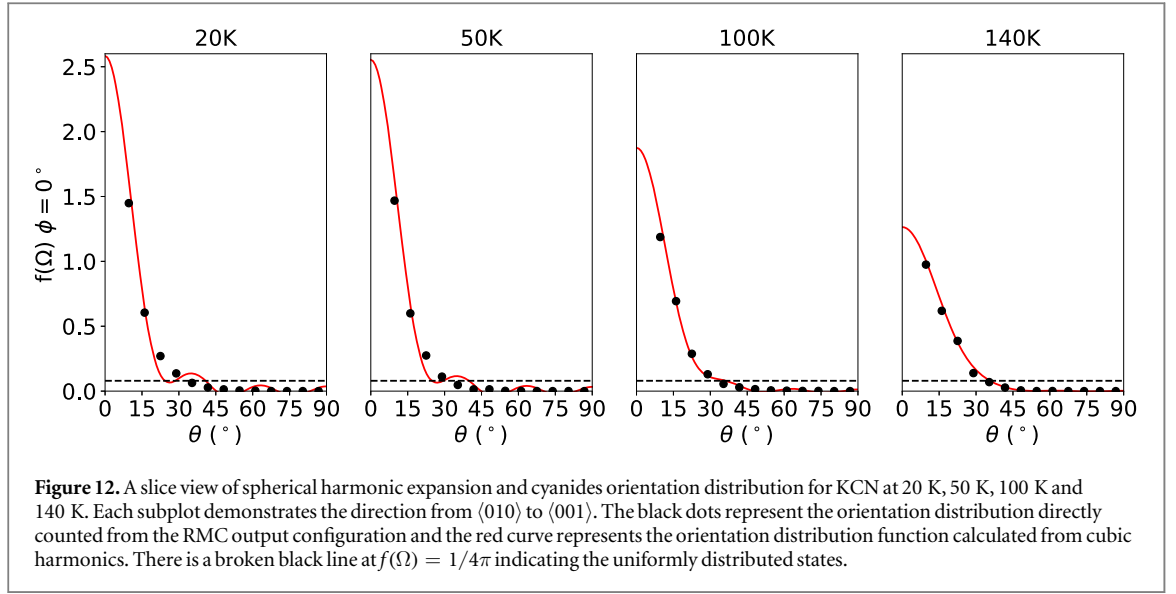| l | 20 K | 50 K |
|---|---|---|
| 1 | −1.6525(2) | −1.6543(1) |
| 2 | 1.9507(7) | −1.881(2) |
| 3 | −2.039(1) | 1.720(3) |
| 4 | 1.993(2) | −1.545(3) |
| 5 | −1.871(3) | 1.369(4) |
| 6 | 1.716(3) | −1.198(4) |
| 7 | −1.554(3) | 1.038(4) |
| 8 | 1.396(4) | −0.892(3) |
| 9 | −1.248(3) | 0.759(3) |
| 10 | 1.110(3) | 1.956(5) |
| 11 | −0.981(3) | −2.048(1) |
| 12 | 0.860(2) | 0.200(2) |

**Table 5.** The values of the coefficients for the $m = 0$ spherical harmonics terms in the bond orientational distribution function for the RMC configurations of the intermediate-temperature *Immm* phase of KCN. By normalisation $c_0 = 1$.

| l | 100 K | 140 K |
|---|---|---|
| 2 | 1.7757(3) | 1.8337(4) |
| 4 | 1.4138(6) | 1.553(1) |
| 6 | 0.756(1) | 0.918(2) |
| 8 | 0.236(2) | 0.419(3) |
| 10 | −0.051(2) | 0.165(2) |
| 12 | −0.143(3) | 0.066(1) |

agreement between histograms of the bond orientation distribution function formed from the atomic configurations with an expansion of the bond orientation distribution function in terms of symmetry-adapted orientational functions. We are able to take the expansion of the distribution function to high order and therefore maintain positive-definiteness, a problem that is encountered when fitting to diffraction data. For future studies of orientational order, we believe that the experience described here should prompt the use of similar methods.

**Figure 12.** A slice view of spherical harmonic expansion and cyanides orientation distribution for KCN at 20 K, 50 K, 100 K and 140 K. Each subplot demonstrates the direction from ⟨010⟩ to ⟨001⟩. The black dots represent the orientation distribution directly counted from the RMC output configuration and the red curve represents the orientation distribution function calculated from cubic harmonics. There is a broken black line at $f(\Omega) = 1/4\pi$ indicating the uniformly distributed states.



**Figure 13.** RMC configurations showing instantaneous orientations of the cyanide anions (top) for one temperature in each of the three phases (250 K for the high-temperature disordered cubic $Fm\bar{3}m$ phase, 100 K for the intermediate-temperature $Immm$ phase, and 20 K for the low-temperature $Pmnm$ phase). The three-dimensional representations of the bond orientation distribution function in each case calculated from the Kubic and spherical harmonics are given in the lower part.

## Appendix. Kubic harmonics

We give here the first five Kubic harmonics in both Cartesian and polar form. Note that the conventional Cartesian form [47] differs by a factor of $\sqrt{4\pi}$ from the polar form given by Bradley and Cracknell [46].

$$K_0 = 1 = \sqrt{4\pi}\,(Y_0^0) \tag{A.1a}$$

$$K_4 = \frac{\sqrt{21}}{4}(5Q - 3) = \sqrt{4\pi}\left(\sqrt{\frac{7}{12}}\,Y_4^0 + \sqrt{\frac{5}{12}}\,Y_4^{4,c}\right) \tag{A.1b}$$

$$K_6 = \frac{\sqrt{13}}{8\sqrt{2}}(462S + 21Q - 17) = \sqrt{4\pi}\left(\sqrt{\frac{1}{8}}\,Y_6^0 - \sqrt{\frac{7}{8}}\,Y_6^{4,c}\right) \tag{A.1c}$$

$$K_8 = \frac{\sqrt{561}}{32}(65Q^2 - 208S - 94Q + 33) = \sqrt{4\pi}\left(\sqrt{\frac{99}{192}}\,Y_8^0 + \sqrt{\frac{28}{192}}\,Y_8^{4,c} + \sqrt{\frac{65}{192}}\,Y_8^{8,c}\right) \tag{A.1d}$$

$$K_{10} = \frac{\sqrt{455}}{64\sqrt{2}}(7106QS + 187Q^2 - 3190S - 264Q + 85) = \sqrt{4\pi}\left( \sqrt{\frac{65}{384}}\, Y_{10}^{0} - \sqrt{\frac{132}{384}}\, Y_{10}^{4,c} - \sqrt{\frac{187}{384}}\, Y_{10}^{8,c} \right)$$

$$(A.1e)$$

In the Cartesian equations, $Q = x^4 + y^4 + z^4$ and $S = x^2 y^2 z^2$, where $x = \sin\theta\cos\phi$, $y = \sin\theta\sin\phi$ and $z = \cos\theta$.

## ORCID iDs

Guanqun Cai ⓘ https://orcid.org/0000-0001-8144-5084
Anthony E Phillips ⓘ https://orcid.org/ 0000-0003-4225-0158
David A Keen ⓘ https://orcid.org/ 0000-0003-0376-2767
Matthew G Tucker ⓘ https://orcid.org/0000-0002-2891-7086
Martin T Dove ⓘ https://orcid.org/0000-0002-8030-1457

## References

[1] Califano S, Schettino V and Neto N 2012 *Lattice Dynamics of Molecular Crystals* vol 26 (Berlin, Heidelberg: Springer) (https://doi.org/10.1007/978-3-642-93186-4)

[2] Vaughan G B M *et al* 1991 Orientational disorder in solvent-free solid $C_{70}$ *Science* **254** 1350–3

[3] Duncan H D, Beake E O R, Playford H Y, Dove M T and Phillips A E 2017 Local structure of a switchable dielectric prussian blue analogue *CrystEngComm* **19** 7316–21

[4] Kanai Y *et al* 2017 Characterization of heme orientational disorder in a myoglobin reconstituted with a trifluoromethyl-group-substituted heme cofactor *Biochemistry* **56** 4500–8

[5] Sakuntala T, Arora A K, Chandra Shekar N V and Ch Sahu P 1998 Orientational disorder: a mechanism of amorphization at high pressure *Europhys. Lett.* **44** 728

[6] Li B *et al* 2019 Colossal barocaloric effects in plastic crystals *Nature* **567** 506

[7] Ong W-L, O'Brien E S, Dougherty P S M, Paley D W, Higgs C F III, McGaughey A J H, Malen J A and Roy X 2017 Orientational order controls crystalline and amorphous thermal transport in superatomic crystals *Nat. Mater.* **16** 83

[8] Lynden-Bell R M, McDonald I R and Klein M L 1983 Analysis of translation-rotation coupling in an orientationally disordered ionic crystal *Mol. Phys.* **48** 1093–117

[9] Collings I E *et al* 2013 Homologous critical behavior in the molecular frameworks Zn(CN)$_2$ and Cd(imidazolate)$_2$ *JACS* **135** 7610–20

[10] Coates C S *et al* 2019 Room temperature spin-ice physics in cadmium cyanide arXiv:1904.05749

[11] Debye P J W 1929 *Polar molecules* (New York: Chemical Catalog Company, Incorporated)

[12] Frenkel J 1935 The liquid state and the theory of fusion. ii. the theory of fusion and crystallization *Acta Phys.-Chim. URSS* **3** 913–38

[13] Press W and Hüller A 1973 Analysis of orientationally disordered structures. i. method *Acta Crystallographica* A **29** 252–6

[14] Dolling G, Powell B M and Sears V F 1979 Neutron diffraction study of the plastic phases of polycrystalline SF$_6$ and CBr$_4$ *Mol. Phys.* **37** 1859–83

[15] Hüller A and Press W 1979 Analysis of orientationally disordered structures. III. positive definiteness of orientational distribution functions *Acta Crystallographica* A **35** 876–80

[16] Gerlach P, Prandl W and Vogt K 2006 The determination of the effective rotational potential in the plastic phase of C$_2$Cl$_6$ from neutron Bragg scattering data *Mol. Phys.* **52** 383–97

[17] Dove M T, Tucker M G and Keen D A 2002 Neutron total scattering method: simultaneous determination of long-range and short-range order in disordered materials *Eur. J. Mineral.* **14** 331–48

[18] Keen D A, Tucker M G and Dove M T 2005 Reverse Monte Carlo modelling of crystalline disorder *J. Phys. Condens. Matter* **17** S15–22

[19] Young C A and Goodwin A L 2011 Applications of pair distribution function methods to contemporary problems in materials chemistry *J. Mater. Chem.* **21** 6464

[20] Beake E O R, Tucker M G, Dove M T and Phillips A E 2017 Orientational disorder in adamantane and adamantanecarboxylic acid *ChemPhysChem* **18** 459–64

[21] Chen T, Foley B J, Ipek B, Tyagi M, Copley J R D, Brown C M, Choi J J and Lee S-H 2015 Rotational dynamics of organic cations in the ch$_3$nh$_3$pbi$_3$ perovskite *Phys. Chem. Chem. Phys.* **17** 31278–86

[22] Even J, Carignano M and Katan C 2016 Molecular disorder and translation/rotation coupling in the plastic crystal phase of hybrid perovskites *Nanoscale* **8** 6222–36

[23] Rowe J M, Rush J J and Prince E 1977 Neutron diffraction study of the structure and phase transitions of alkali cyanide crystals *J. Chem. Phys.* **66** 5147–9

[24] Price D L, Rowe J M, Rush J J, Prince E, Hinks D G and Susman S 1972 Single crystal neutron diffraction study of potassium cyanide *J. Chem. Phys.* **56** 3697–702

[25] Impey R W, Sprik M and Klein M L 1985 Simulation of the cubic to orthorhombic phase transition in potassium cyanide *J. Chem. Phys.* **83** 3638–44

[26] Michel K H and De Raedt H 1976 Unified rotational dynamics of molecular crystals with orientational phase transition *J. Chem. Phys.* **65** 977–84

[27] Michel K H and Naudts J 1977 Anomalous thermoelastic behavior and molecular reorientations in crystals *J. Chem. Phys.* **67** 547–58

[28] Michel K H and Naudts J 1978 Dynamics of translations and rotations in molecular crystals *J. Chem. Phys.* **68** 216

[29] Rowe J M, Rush J J, Chesser N J, Michel K H and Naudts J 1978 Nature of the phase transition in KCN at 168 K *Phys. Rev. Lett.* **40** 455–8

[30] Sharma R M and Sharma T P 1987 Lattice dynamics of KCN *J. Phys. C: Solid State Phys.* **20** 3411–6

[31] Lynden-Bell R M and Michel K H 1994 Translation-rotation coupling, phase transitions, and elastic phenomena in orientationally disordered crystals *Rev. Mod. Phys.* **66** 721–62

[32] Stokes H T, Decker D L, Nelson H M and Jorgensen J D 1993 Structure of potassium cyanide at low temperature and high pressure determined by neutron diffraction *Phys. Rev.* B **47** 11082

[33] Durand D, do Carmo L C S, Anderson A and Lüty F 1980 Raman and infrared studies of rotational-translational modes in stress-aligned ferroelastic kcn and nacn *Phys. Rev.* B **22** 4005

[34] Powell B M 1990 Neutron scattering at Chalk river *Neutron News* **1** 16–20

[35] Hannon A C 2005 Results on disordered materials from the general materials diffractometer, GEM, at ISIS *Nucl. Instrum. Methods Phys. Res., Sect. A* **551** 88–107

[36] Arnold O *et al* 2014 Mantid–data analysis and visualization package for neutron scattering and $\mu$ SR experiments *Nuclear Inst. and Methods in Physics Research, A* **764** 156–66

[37] Larson A C and Von Dreele R B 2004 General structure analysis system (GSAS) *Technical Report*, Los Alamos National Laboratory LAUR 86–748

[38] Toby B H 2001 Expgui, a graphical user interface for gsas *J. Appl. Crystallogr.* **34** 210–3

[39] Toby B H and Von Dreele R B 2013 GSAS-II: the genesis of a modern open-source all purpose crystallography software package *J. Appl. Crystallogr.* **46** 544–9

[40] Keen David A. 2001 A comparison of various commonly used correlation functions for describing total scattering *Journal of Applied Crystallography* **34** 172–77

[41] Soper Alan 2011 *GudrunN and GudrunX : programs for correcting raw neutron and X-ray diffraction data to differential scattering cross section* RAL-TR-2011-013 Rutherford Appleton Laboratory

[42] Tucker M G, Keen D A, Dove M T, Goodwin A L and Hui Q 2007 RMCProfile: reverse Monte Carlo for polycrystalline materials *J. Phys. Condens. Matter* **19** 335218

[43] Dove M T and Rigg G 2013 RMCgui: a new interface for the workflow associated with running reverse Monte Carlo simulations *J. Phys. Condens. Matter* **25** 454222454222–9

[44] Carpenter M A, Becerro A I and Seifert F 2001 Strain analysis of phase transitions in $(Ca,Sr)TiO_3$ perovskites *Am. Mineral.* **86** 348–63

[45] Stokes H T and Hatch D M 2002 Copl: program for obtaining a complete list of order parameters for a group-subgroup crystalline phase transition *J. Appl. Crystallogr.* **35** 379–379

[46] Bradley C and Cracknell A 2009 *The Mathematical Theory of Symmetry in Solids: Representation Theory for Point Groups and Space Groups* (Oxford: Oxford University Press)

[47] Fehlner W R and Vosko S H 1976 A product representation for cubic harmonics and special directions for the determination of the Fermi surface and related properties *Can. J. Phys.* **54** 2159–69

[48] Rowe J M, Hinks D G, Price D L, Susman S and Rush J J 1973 Single crystal neutron diffraction study of sodium cyanide *J. Chem. Phys.* **58** 2039–42